Smart Education System Enhancing Collaborative Learning with Virtual Reality and Cloud-Edge Computing Task Scheduling Algorithm

Guirong Li[1*] and Lei Shu[2]

[1, 2]Guangdong University of Finance & Economics, Gangzhou, 510320, China
[1]kirro@gdufe.edu.cn, [2]leishu.2023@163.com

Corresponding author: Guirong Li, kirro@gdufe.edu.cn

Abstract. In order to improve the resource scheduling effect of the smart education system (SES), this paper combines the cloud- edge collaborative task scheduling algorithm to process the resource scheduling of the smart education model, and proposes a closed-loop system load modeling method based on the small disturbance data measured by the PMU. The closed-loop system load modeling method proposed in this paper improves the previous load modeling method, and further improves the load modeling method based on the overall measurement method. In addition, this paper constructs the system architecture based on the resource scheduling requirements of the SES. The experimental research shows that the SES based on the cloud- edge collaborative computing task scheduling algorithm can effectively improve the effect of cloud computing education resource scheduling (CCERS).

Keywords: cloud-edge collaborative computing; task scheduling; smart education; system resources; Virtual Reality
DOI: https://doi.org/10.14733/cadaps.2023.S14.50-71

1 INTRODUCTION

At present, the more mature algorithms aiming at performance (such as optimal span, earliest completion time of tasks, etc.) mainly include Max-Min algorithm, Min-min algorithm, ant colony algorithm, genetic algorithm, greedy algorithm and simulated annealing algorithm. Some scholars also put forward some strategies for the scheduling performance of cloud computing platforms. In the literature [3], the author proposes a genetic algorithm with dual fitness based on the MapReduce model. In the literature [1], the author studies the load balancing scheduling algorithm of cloud computing resources based on the minimum migration cost.

At present, some foreign companies have researched and applied these algorithms. For example, IBM has built a cloud computing platform that adopts a performance-oriented scheduling method; Intel has proposed a model for predicting the competition of virtual resources [15]; Reference [5] Adopt a two-level scheduling method to perform integrated management on virtual machines to

provide scheduling services to users. The quality of service provided by cloud computing is related to its sustainable development. Currently, cloud computing task scheduling mainly considers the following quality of service parameters: cost, time, reliability, and bandwidth. Reference [8] takes network bandwidth as one of the indicators to measure service quality, selects resources through weighted average, assigns different priorities to different tasks, and prioritizes tasks with higher priority; Reference [2] analyzes the According to the different requirements of QoS, a multi-QoS scheduling strategy based on multiple workflows. Cloud computing is a business computing model, and the economic factor is an important goal of its operation [11]. The HP cloud computing data center prioritizes costs and provides services centered on economic principles; Literature [17] proposes a market-oriented cloud computing architecture and resource allocation and scheduling methods, through SLA (Service-Level Agreement) resource allocation The reference [12] proposes a scheduling strategy based on computing intensity. Users with higher computing power or real-time requirements can choose resources with stronger computing power, while Users with lower requirements can choose resources with weak computing power to reduce the cost of cloud services.

In fact, many researches on scheduling strategies will take into account various factors, such as users' QoS requirements, scheduling performance and economic indicators. The cloud computing scheduling strategy of Reference [18] considers user QoS requirements, load balancing, reliability and cost at the same time; Reference [4] proposes a resource scheduling method based on a continuous two-way auction mechanism, which takes into account both users and service providers. benefits, such as completion time, cost, resource utilization and throughput, etc. Reference [20] proposed a multi-objective hybrid genetic algorithm, taking into account both energy consumption and completion time. At this stage, there are more and more mature researches on task scheduling algorithms in cloud computing, but these algorithms are more suitable for general cloud computing platforms. Education cloud belongs to the category of cloud computing. It has many characteristics of traditional cloud computing. Since it is called education, the cloud also has its differences from general cloud computing.

The education cloud enables teachers to teach effectively and students to learn actively. Cloud computing-assisted education CCBE, also known as "cloud computing-based education"[14]. For a mesh, it should never be assumed that it is immutable. Originally owned resources or functions may fail or become unavailable at the next moment; and previously unavailable resources may be added over time [19]. The number of users, resources and services in the grid environment is huge, so the grid should adapt to large-scale dynamic changes in terms of performance, functions, management software, and compatibility. The dynamics of grid includes two aspects: dynamic increase and dynamic decrease. The characteristics of dynamic changes of grid resources require grid management to fully consider and solve this problem. For the dynamic reduction of grid resources or resource failures, grids are required to take timely measures to realize automatic task migration. To be transparent to high-level users or minimize user losses. The dynamic increase of grid resources needs to improve the flexibility and scalability of the grid, that is to say, in the design and implementation of the grid, it must be considered whether new resources can be added to the grid naturally and flexibly. , and can be integrated with the original resources to play a role together [16].

Grid resources are heterogeneous and diverse. Grid's resources are not only geographically dispersed, but also vary widely in form and content. The grid must be built on a variety of heterogeneous resources to solve the communication and interoperability problems between these different structures and different types of resources. It is precisely because of the existence of heterogeneity or resource diversity that a greater challenge is put forward to the design of grid software. Only by solving this problem can grids be more attractive [10].

The resources on the grid first belong to a certain organization or individual. Therefore, the owner of the grid resource has the highest level of management authority for the resource. The grid should allow the resource owner to have the ability to independently manage his resources. This is the autonomy of the grid. However, grid resources must also be managed uniformly by grids, otherwise

different resources will not be able to establish mutual connections, share and interoperate, and cannot provide convenient services for more users as a whole [7].

The construction of educational resources can have four levels of meanings: one is the construction of material-based educational resources; the other is the construction of online courses; the third is the evaluation of resource construction; the fourth is the development of educational resource management systems. Among these four levels, material-based educational resources and online course construction are the foundation, and are the focus and core that needs to be standardized; the third level is the evaluation and screening of resources, and the standards for evaluation need to be standardized; the fourth level is The construction of the tool level, the specific content of material education resources and online courses are ever-changing, and the forms have their own characteristics. The corresponding management system must adapt to the changes in this form and make full use of their characteristics. The construction of educational resources is a systematic project, which involves systematic engineering of teaching theories, teaching concepts, teaching contents, teaching strategies, technical specifications, etc. Network companies, publishing houses and other aspects of the extensive participation, joint construction [13].

Because the construction of educational resources is not a one-step process, but a dynamic process of "lack-supply-balance-lack-supply...", coupled with the basic education curriculum reform, many personalized educational resources have been born [6]. With the improvement of education level and the increasing demand for education, the construction of educational resources should be continuously improved and updated to meet the development requirements of the times. Long-term and stable continuous updating and maintenance is the guarantee for the lasting vitality of educational resources [9].

This paper combines the cloud-edge collaborative computing (CCC)task scheduling algorithm to perform resource scheduling processing of the smart education model to improve the stable operation of the education system.

2 LOAD MODELING METHOD OF SES BASED ON SMALL DISTURBANCE DATA MEASURED BY PMU

2.1 Closed-loop System for Load Model Identification

Ignoring the influence of frequency, the model of the SES network is shown in formula (1)

$$\dot{x}_1(t) = A_1 x_1(t) + B_1 u_1(t) + L_1 e_1(t)$$
$$y_1(t) = C_1 x_1(t) + D_1 u_1(t) \tag{1}$$

In the formula, $L_1 e_1(t)$ is the noise input of other nodes, that is, external disturbance, $y_1(t)$ is the data load of the node where the load to be identified is located, $u_1(t)$ is the active power and reactive power (APRP) of the node where the load to be identified is located, including the response output and time-varying random switching disturbance of the load to be identified. In order to facilitate the unified representation, the load model shown in formula (13) is written in the following form:

$$\dot{x}_2(t) = A_2 x_2(t) + B_2 u_2(t) + L_2 e_2(t)$$
$$y_2(t) = C_2 x_2(t) + D_2 u_2(t) \tag{2}$$

In the formula, $L_2 e_2(t)$ is the time-varying random switching disturbance of the load to be identified, that is, the internal disturbance, $y_2(t)$ is the APRP of the node where the load to be identified is located, and $u_2(t)$ is the data load of the node where the load to be identified is located. $y_2 = u_1, y_1 = u_2$ needs to be noted.

From formula (1) and formula (2), the transfer function model of the network and load of the SES can be obtained.

$$y_1(t) = C_1 (sI - A_1)^{-1} B_1 u_1(t) + C_1 (sI - A_1)^{-1} L_1 e_1(t)$$
$$= C(s) u_1(t) + H_1(s) e_1(t) \tag{3}$$

$$y_2(t) = C_2 (sI - A_2)^{-1} B_2 u_2(t) + C_2 (sI - A_2)^{-1} L_2 e_2(t)$$
$$= G(s) u_2(t) + H_2(s) e_2(t) \tag{4}$$

It can be seen that the data load changes of load nodes are driven by all load fluctuations. Since the data sampled in practice is discrete, the above system is transformed to obtain the closed-loop system as shown in Figure 1.
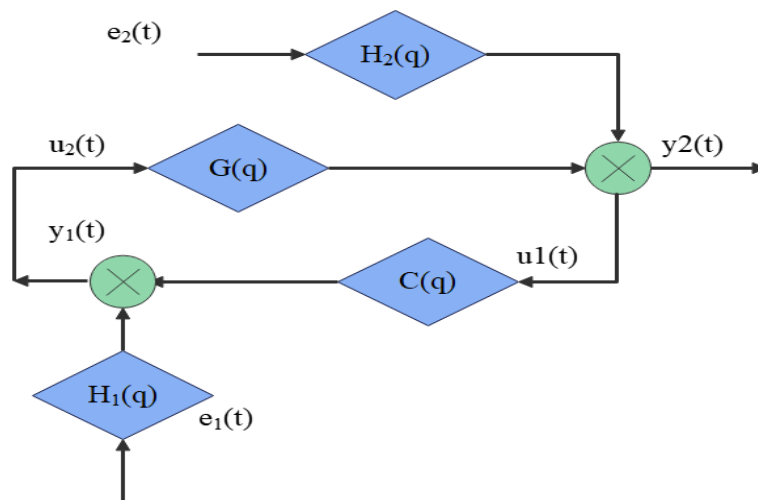

Figure 1: Load modelling closed-loop system.

Among them, G(q) is the load model to be identified, C(q) is the network model of the SES, e1(t) is the switching noise of the remaining load nodes, and e2(t) is the switching noise of the load nodes to be identified.

2.2   Dentifiability Analysis of Load Model

The data load amplitude, APRP collected by the PMU constitute a data set, and the data set should have the ability to distinguish two different load models. For the convenience of research, the closed-loop system shown in Figure 1 is written in the form of formula (5).

$$y_2(t) = S_0(q)H_1(q)G(q)\xi_1(t) + S_0(q)H_2(q)\xi_2(t)$$
$$u_2(t) = S_0(q)H_2(q)C(q)\xi_2(t) + S_0(q)H_1(q)\xi_1(t)$$

(5)

In the formula, $S_0(q)$ is the sensitivity function.

$$S_0(q) = \frac{1}{1 - G(q)C(q)}$$

(6)

We assume that two load models, W_1 and W_2, are identified using the quasi-stationary data set Z^N. If the identification result is accurate, obviously the two load models should be the same, namely $W_1 \equiv W_2$, as shown in formula (7).

$$\bar{E}\left\{[W_1(q) - W_2(q)]z(t)\right\}^2 = 0$$

(7)

In the formula, $\bar{E}x = \lim \frac{1}{N}\sum_{t=1}^{N} Ex(t)$. Because of $W_1(q) - W_2(q) = \left[\Delta W_u(q), \Delta W_y(q)\right]$, formula (7) can be written in the following form:

$$\bar{E}\left[\Delta W_u u_2(t) + \Delta W_y y_2(t)\right]^2 = 0$$

(8)

In the formula, $\Delta W_u = W_u(q, \theta_1) - W_u(q, \theta_2), \Delta W_y = W_y(q, \theta_1) - W_y(q, \theta_2)$. If formula (5) is substituted into formula (8), there is:

$$\bar{E}\left[\left(\Delta W_u + G\Delta W_y\right)S_0 H_1 e_1 + \left(\Delta W_y + C\Delta W_u\right)S_0 H_2 e_2\right]^2 = 0$$

(9)

In the formula, e_1 and e_2 are the combination of uncorrelated random disturbance signals after filtering. Since the filter is stable full rank, the spectral densities of H_1 and H_2 are always greater than zero. Therefore, if the feedback channel satisfies:

$$C \neq \frac{\Delta W_y}{\Delta W_u}$$

(10)

Then, $\Delta W_y = \Delta W_u = 0$, namely $W_1 = W_2$, can be deduced, indicating that the load model can be identified. Therefore, when the feedback controller has higher-order, nonlinear or time-varying characteristics, the load model can be identified. In the closed-loop system of load modeling, the feedback channel is the network model of the SES, so the feedback controller is complex enough to ensure sufficient information in the data set.

In addition, in order to more intuitively judge whether the data set has sufficient information, power spectrum analysis can be performed on the data set. We set $W_1(q) - W_2(q) = \tilde{W}(q)$, and formula (7) is equivalent to formula (11).

$$\int_{-\pi}^{\pi} \tilde{W}\left(e^{i\omega}\right) \Phi_Z(\omega) \tilde{W}^T\left(e^{-i\omega}\right) d\omega = 0 \tag{11}$$

In the formula, $\Phi_Z(\omega)$ is the spectral matrix of $Z(t) = [u(t), y(t)]^T$

$$\Phi_z(\omega) = \begin{bmatrix} \Phi_u(\omega) \Phi_{uy}(\omega) \\ \Phi_{yu}(\omega) \Phi_y(\omega) \end{bmatrix} \tag{12}$$

When $\Phi_Z(\omega) \neq 0$, $W_1(q) - W_2(q) = \tilde{W}(q) = 0$ is satisfied. Therefore, the condition for sufficient information for data set Z^∞ is that the spectral matrix of Z(t).

When solving the parameters of the load model, there may be multiple solutions or no solutions, and the continuous excitation of the data set can make the solution results of the parameters unique. When using the forecast error method to identify the parameters of the n-order load model, the input signal needs to be n-order continuous excitation. Specifically, we assume that the input sequence is $u(k), k = 0, 1, 2, 3 \cdots$. When there is an integer N such that the matrix (13) is full of rank, then u(k) is said to be a continuous excitation of order n.

$$U = \begin{bmatrix} u(0)u(1)\cdots u(N-1) \\ u(1)u(2)\cdots u(N) \\ \vdots \vdots \ddots \vdots \\ u(n-1)u(n)\cdots u(N+n-2) \end{bmatrix} \tag{13}$$

The condition of continuous excitation is equivalent to the matrix non-singularity of formula (14).

$$R^u = \lim_{N \to \infty} \frac{1}{N} \sum_{i=1}^{N} UU^T$$

$$= \begin{bmatrix} R_u(0)R_u(1)\cdots R_u(n-1) \\ R_u(-1)R_u(0)\cdots R_u(n-2) \\ \vdots \vdots \ddots \vdots \\ R_u(1-n)R_u(2-n)\cdots R_u(0) \end{bmatrix} \tag{14}$$

The identifiability of the load model structure is related to the reversibility of the load model structure $\mathcal{M}$. That is, if the load model structure $\mathcal{M}$ is full shot, the load model structure can be identified. For the convenience of expression, the coefficient matrix of formula (15) is denoted as:

$$A = \begin{bmatrix} a_{11}a_{12}a_{13} \\ a_{21}a_{22}a_{23} \\ 0a_{32}0 \end{bmatrix}, C = \begin{bmatrix} 0c_{12}0 \\ c_{21}00 \end{bmatrix}$$

$$B = \begin{bmatrix} b_{11} \\ 0 \\ b_{31} \end{bmatrix}, D = \begin{bmatrix} d_{11} \\ d_{21} \end{bmatrix}$$

(15)

In the process of solving the parameters, only the load model is concerned, the noise model is ignored, and the load transfer function model of formula (16) is recorded as

$$\Delta P = \frac{B_{0p}s^3 + B_{1p}s^2 + B_{2p}s + B_{3p}}{s^3 + A_1 s^2 + A_2 s + A_3} \Delta V$$

$$\Delta Q = \frac{B_{0q}s^3 + B_{1q}s^2 + B_{2q}s + B_{3q}}{s^3 + A_1 s^2 + A_2 s + A_3} \Delta V$$

(16)

If the structure of the load model used in this paper is identifiable.

According to the conversion relationship $G(s) = C(sI - A)^{-1}B + D$ between the transfer function model and the state space model, it can be obtained from formulas (15) and (16).

$$A_1 = -(a_{11} + a_{22}), A_2 = a_{11}a_{22} - a_{12}a_{21} - a_{23}a_{32}, A_3 = a_{11}a_{23}a_{32} - a_{13}a_{21}a_{32}$$

$$B_{0p} = d_{11}, B_{1p} = d_{11}A_1, B_{2p} = d_{11}A_2 + a_{23}b_{31}c_{12} + a_{21}b_{11}c_{12}$$

$$B_{3p} = d_{11}A_3 + b_{31}c_{12}(a_{13}a_{21} - a_{11}a_{23}), B_{0q} = d_{21}, B_{1q} = d_{21}A_1 + b_{11}c_{21}$$

$$B_{2q} = d_{21}A_2 + a_{13}b_{31}c_{12} - a_{22}b_{11}c_{21}, B_{3p} = d_{21}A_3 + b_{31}c_{12}(a_{12}a_{23} - a_{13}a_{22}) - b_{11}c_{21}a_{23}a_{32}$$

(17)

Because of $a_{11} = a_{22}, a_{12} = -a_{21}, c_{12} = c_{21}, a_{32}a_{13} = b_{31}V_0$, after sorting out the formula (17), it is found that the value of the parameter $a_{11}, a_{22}, d_{11}, d_{21}$ can be directly obtained without additional conditions, while other parameters can only obtain the relationship between each other, and the value of each parameter cannot be accurately obtained.

2.3 Load Modeling Method of Closed-loop System

Firstly, the load amplitude sequence V(k), the active power sequence P(k) and the reactive power sequence Q(K) with the total sequence length N are selected from the small disturbance data measured by the PMU, and the measured data of the PMU are converted into standard values. Since the SES is a nonlinear system, the data can be used to identify the linear system after de-averaging.

The preprocessed data is denoted as $Z = \{ \Delta P(k), \Delta Q(k), \Delta V(k) \}, k = 1, 2, 3 \cdots N$.

In this paper, the appropriate load model order is selected by comparing the fitting degree between the response output of the load model of different orders and the network operation data of the SES measured by the PMU. The above degree of fit is measured by the error sum of squares function, and the specific expression is shown in formula (18).

$$J(n) = \sum_{k=n+1}^{N+n} e^T(k)e(k) = \left(Y - \phi\hat{\theta}_n\right)^T \left(Y - \phi\hat{\theta}_n\right)$$

(18)

In the formula, $\hat{\theta}_n$ is the estimated value of the parameters of the load model of order n. In general, J(n) decreases as n increases. However, when n increases to be larger than the actual order, the decrease of J(n) is not obvious, and the relationship between J(n) and n presents an L-shaped curve. For the convenience of expression, the input $\Delta V(k)$ is denoted as u(t), and the outputs $\Delta P(k)$ and $\Delta Q(k)$ are denoted as y(t). We assume that the true load model is shown in formula (19).

$$y(t) = \frac{B_0(q)}{A_0(q)}u(t) + \frac{C_0(q)}{D_0(q)}e(t) = G_0(q)u(t) + H_0(q)e(t)$$

(19)

The above model is the Box-Jenkins (BJ) model. According to the principle of the forecast error method introduced, the forecast value and single-step forecast error of the model are shown in formula (20) and formula (21), respectively.

$$\hat{y}(t,\theta) = H^{-1}(q)G(q)u(t) + \left[1 - H^{-1}(q)\right]y(t)$$

(20)

$$\varepsilon(t,\theta) = y(t) - \hat{y}(t/t-1) = -H^{-1}(q)[G(q)u(t) - y(t)]$$

(21)

A set of optimal parameter vectors θ are sought to minimize the sum of the single-step prediction errors, that is, the loss function V_{BJ} is the smallest. The expression of the loss function is shown in formula (22).

$$V_{BJ} = \frac{1}{N}\sum_{t=1}^{N}\varepsilon^2(t,\theta) = \frac{1}{N}\sum_{t=1}^{N}\left\{H^{-1}(q)[y(t) - G(q)u(t)]\right\}^2$$

(22)

Since the relationship between the loss function V_{BJ} and the parameters of A(q) is nonlinear, it is necessary to solve the load model parameters by numerical optimization algorithm. $\hat{\theta}_k$ is the estimated value of the k-th iteration, the one-step forecast error is approximated by ignoring the higher-order terms in the Taylor expansion, namely:

$$\varepsilon(t,\theta) \approx \varepsilon\left(t,\hat{\theta}_k\right) + \left.\frac{\partial\varepsilon(t,\theta)}{\partial\theta^T}\right|_{\theta=\hat{\theta}_k} \left(\theta - \hat{\theta}_k\right) = \varepsilon\left(t,\hat{\theta}_k\right) + \varphi^k(t)\left(\theta - \hat{\theta}_k\right)$$

(23)

$$\varphi^k(t) = \left[\frac{\hat{B}^k(q)}{\hat{A}^k(q)^2}u(t-1)\cdots\frac{\hat{B}^k(q)}{\hat{A}^k(q)^2}u(t-n)\frac{-1}{\hat{A}^k(q)}u(t-1)\cdots\frac{-1}{\hat{A}^k(q)}u(t-n)\right]$$

(24)

$$\hat{\theta}_N = \left\{ \sum_{t=1}^{N} \varphi^k(t)\left[\varphi^k(t)\right]^T \right\}^{-1} \sum_{t=1}^{N} \varphi^k(t)\left[\varphi^k(t)\right]^T \left[\hat{\theta}_k - \varepsilon\left(t,\hat{\theta}_k \right)\right] \tag{25}$$

The above algorithm needs to satisfy two conditions. One is that the model obtained by each iteration must be a stable model, and the other is that $\hat{A}^k(q)$ and $\hat{B}^k(q)$ are relatively prime. For the parameter identification of the load model, these two conditions are easy to satisfy.

Therefore, the load BJ model can be identified.

$$\Delta P = \frac{B_p(q)}{A_p(q)}\Delta V + \frac{C_p(q)}{D_p(q)}\Delta e(t)$$

$$\Delta Q = \frac{B_q(q)}{A_q(q)}\Delta V + \frac{C_q(q)}{D_q(q)}\Delta e(t) \tag{26}$$

The following steps are required to convert the load BJ model established by the method proposed in this paper into the proposed comprehensive load model. (1) The load BJ model is converted into a load discrete transfer function model. (2) The load discrete transfer function model is converted into a load continuous transfer function model; (3) The high-order load continuous transfer function model is converted into a third-order load continuous transfer function model. These steps are described in detail below.

1) The load BJ model is converted into a load discrete transfer function model. The load BJ model identified by formula (26) is Z-transformed, and the load discrete transfer function model is obtained.

$$\Delta P(z) = \frac{B_{pu}(z)}{A(z)}\Delta V(z) = H_{pu}(z)\Delta V(z)$$

$$\Delta Q(z) = \frac{B_{qu}(z)}{A(z)}\Delta V(z) = H_{qu}(z)\Delta V(z) \tag{27}$$

In the formula,

$$A(z) = z^n + \sum_{i=1}^{n} a_i z^{n-i}, B_{pu}(z) = \sum_{i=0}^{mp} b_{pi} z^{n-i}, B_{qu}(z) = \sum_{i=0}^{mq} b_{qi} z^{n-i} \tag{28}$$

$H_{pu}(z)$ and $H_{qu}(z)$ are discrete transfer function matrices.

2) The load discrete transfer function model is converted into a load continuous transfer function model

Using bilinear variation, formula (28) can be transformed into a load continuous transfer function model. For the convenience of writing, $H_{pu}(z)$ and $H_{qu}(z)$ are written uniformly as:

$$H_0(z) = \frac{b_0 z^m + b_1 z^{m-1} + \cdots + b_m}{z^n + a_1 z^{n-1} + \cdots + a_n}$$

(29)

We set:

$$z = \frac{1 + \frac{h}{2}S}{1 - \frac{h}{2}S}$$

(30)

Then the transfer function can be found.

$$G(S) = \frac{\sum_{i=0}^{m} b_i \left(1 + \frac{h}{2}S \right)^{m-i} \left(1 - \frac{h}{2}S \right)^{i}}{\sum_{i=1}^{n} a_i \left(1 + \frac{h}{2}S \right)^{n-i} \left(1 - \frac{h}{2}S \right)^{i}}$$

(31)

By Newton's expansion

$$\left(1 + \frac{h}{2}S \right)^{n-i} \left(1 - \frac{h}{2}S \right)^{i} = \sum_{j=0}^{n} \left[\sum_{l=0}^{j} C_i^l C_{n-i}^{j-l} (-1)^l \right] \left(\frac{h}{2} \right)^{j} S^{j}$$

(32)

The continuous transfer function can be further derived.

$$G(S) = \frac{\sum_{j=0}^{m} \beta_j S^{m-j}}{S^n + \sum_{j=1}^{n} \alpha_j S^{n-j}}$$

(33)

In the formula,

$$\alpha_j = \frac{\sum_{i=1}^{n} a_i \left[\sum_{l=0}^{j} (-1)^l C_i^l C_{n-i}^{j-l} \right] + C_n^j}{\sum_{i=1}^{n} a_i \left[\sum_{l=0}^{n} (-1)^l C_i^l C_{n-i}^{n-l} \right] + 1} \left(\frac{h}{2} \right)^{j-n}$$

$$\beta_j = \frac{\sum_{i=1}^{m} b_i \left[\sum_{l=0}^{j} (-1)^l C_i^l C_{m-i}^{j-l} \right] + b_0 C_m^j}{\sum_{i=1}^{n} a_i \left[\sum_{l=0}^{n} (-1)^l C_i^l C_{n-i}^{n-l} \right] + 1} \left(\frac{h}{2} \right)^{j-n}$$

(34)

By performing bilinear transformation on $H_{pu}(z)$ and $H_{qu}(z)$ respectively, the load continuous transfer function model can be obtained.

$$\Delta P = \frac{\sum_{j=0}^{mp}\beta_j S^{mp-j}}{S^n + \sum_{j=1}^{n}\alpha_j S^{n-j}}\Delta V = G_{pu}(S)\Delta V$$

$$\Delta Q = \frac{\sum_{j=0}^{mq}\beta_j S^{mq-j}}{S^n + \sum_{j=1}^{n}\alpha_j S^{n-j}}\Delta V G_{qu}(S)\Delta V$$

(35)

3) The high-order load continuous transfer function model is converted into a third-order load continuous transfer function model

The load models established by order selection are generally higher than the third order, and the actual load model is higher than the third order. Therefore, it is generally necessary to reduce the model order in the load model conversion. The load model is reduced by the equilibrium truncation method, which is divided into the following five steps.

1) The continuous transfer function model is converted into the corresponding continuous state space model, and the fully controllable Gram matrix P and the fully observable Gram matrix Q are obtained by Lyapnov equations $AP + PA^T + BBT^T = 0$ and $A^TQ + QA + C^TC = 0$ .1.

2) The balanced transformation matrix T of the system to be solved. The matrix P is subjected to Cholesky decomposition $P = R^TR$, where R is an upper triangular matrix, and $RQRR^T$ is subjected to SVD decomposition to obtain:

$$RQR^T = U\Sigma^2 \, diag\left\{\sigma_1 I_{n1},\sigma_2 I_{n2},\cdots,\sigma_k I_{nk}\right\} U^T$$

(36)

In the formula, $\sum_{i=1}^{k} n_i = n$, and $T = R^T U \Sigma^{-\frac{1}{2}}$, then T is the balance transformation matrix of the system.

3) The original system is reduced to a third-order system, and $\tilde{P}_3 = Q_3 = diag\left\{\sigma_1 I_{n1},\sigma_2 I_{n2},\cdots,\sigma_r I_{nr}\right\}$, where $\sum_{i=1}^{r} n_i = 3$, and then the matrix A, B, C is divided into blocks

$$A = \begin{bmatrix} A_{11} A_{12} \\ A_{21} A_{22} \end{bmatrix} B = \begin{bmatrix} B_{11} \\ B_{21} \end{bmatrix} C = \begin{bmatrix} C_{11} C_{12} \end{bmatrix}$$

(37)

In the formula, $A_{11} \in R^{3 \times 3}, B_{11} \in R^{3 \times 1}, C_{11} \in R^{3 \times 3}$. If $A = A_{11}, B = B_{11}, C = C_{11}, D = D$, then the 3rd order system $\{A, B, C, D\}$ is obtained.

4. The load third-order continuous transfer function model is obtained from $G(s) = C^T(SI - A)^{-1}B + D$

$$\Delta P = \frac{b_{0p}s^3 + b_{1p}s^2 + b_{2p}s + b_{3p}}{s^3 + a_1s^2 + a_2s + a_3} \Delta V$$

$$\Delta Q = \frac{b_{0q}s^3 + b_{1q}s^2 + b_{2q}s + b_{3q}}{s^3 + a_1s^2 + a_2s + a_3} \Delta V$$

(38)

3 SES BASED ON CCC TASK SCHEDULING ALGORITHM

SES based on CCC task scheduling algorithm is shown in figure 2. After identifying the load model, the validity of the load model should be verified. The main verification methods are the fit test between the response output of the load model and the actual data of the SES network, the residual test, and the test of the transient parameters of the load model.
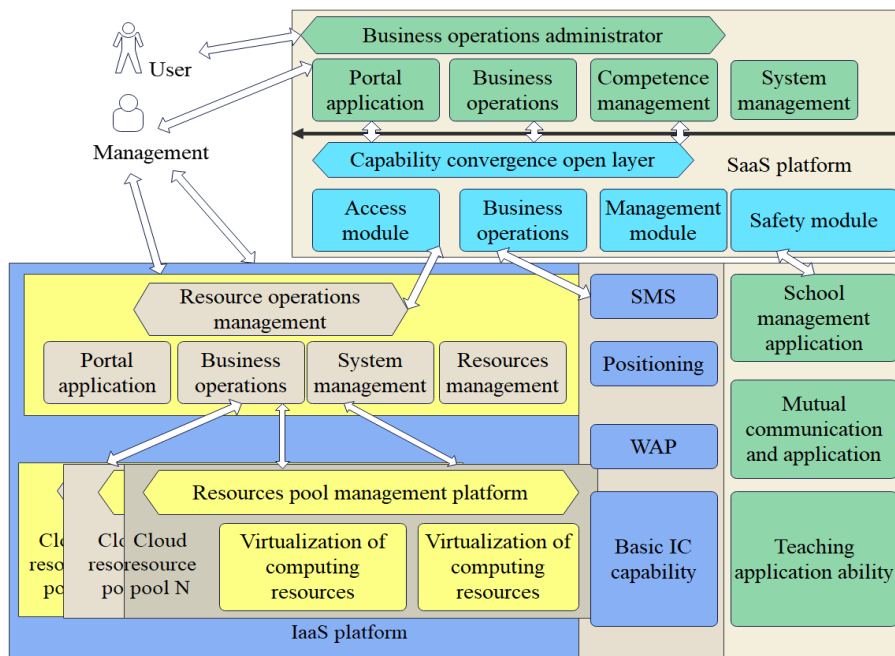
Figure 2: SES based on CCC task scheduling algorithm.

1) Fit test

The normalized root mean square error (NRMSE) is used to represent the fitting degree between the response output of the load model and the actual data of the SES network. The expression of fitting degree is shown in formula (39).

$$fit = 100 \times \left(1 - \frac{\| y - \hat{y} \|}{\| y - mean(\, y\,) \|} \right)$$

(39)

The higher the fitting degree, the closer the response output of the identified load model is to the actual data of the SES network, and the closer the identified load model is to the actual load model in the SES network. It is important to note that the fit test should use a cross test, namely, the data set is divided into two parts. One part is used to estimate the model and the other part is used to validate the model, which avoids the problem of overfitting the data.

2) Residual analysis

The residual is the difference between the actual data of the SES network and the identified response output value of the load model, namely:

$$\varepsilon(\, t\,) = \varepsilon(\, t, \hat{\theta}\,) = y(\, t\,) - \hat{y}(\, t, \theta\,)$$

(40)

If the assumptions are met, the identified load model is more consistent with the real load model of the smart education system network.

For assumption (1), a residual whiteness test is required. The autocorrelation function of the residual is shown in formula (41).

$$\hat{R}_{\varepsilon}(\, \tau\,) = \frac{1}{N} \sum_{t=1}^{N} \varepsilon(\, t\,)\varepsilon(\, t - \tau\,)$$

(41)

The value of $\hat{R}_{\varepsilon}(\, \tau\,)$ is zero when $\tau \neq 0$. Such requirements are very strict and difficult to meet in practice. Therefore, the condition can be relaxed as if $\hat{R}_{\varepsilon}(\, \tau\,)$ is close to zero at $\tau \neq 0$, the residual $\varepsilon(\, t\,)$ can be considered as white noise.

For assumption (2), a residual independence test is required. A good load model should have residuals that are uncorrelated with past inputs. If the residuals are related to the past input, it means that the load model does not describe the relationship between a part of the output and the corresponding input. In the case of feedback, the residual is related to the future input, so in the closed-loop system, pay attention to the positive lag of the cross-correlation function between the residual and the input. In the case of feedback, the residual is related to the future input.

$$\hat{R}_{\varepsilon u}(\, \tau\,) = \frac{1}{N} \sum_{t=1}^{N} \varepsilon(\, t\,)u(\, t - \tau\,), \tau = 1, 2, \cdots$$

(42)

3) Numerical test of load transient parameters

The order of the load model is selected. The expression of the load BJ model is shown in formula (26), and the order na and nb of the denominator A(q) and the numerator B(q) of the load model take integer values from 1 to 10, respectively. Figure 3 shows the relationship between the order of the load model of the education branch system 1 and the sum of squares of errors. The abscisa of

Figure 3(a) is the sum of the orders of the load active power model, namely $n_{ap} + n_{bp}$, and the

abscissa of Figure 3(b) is the sum of the orders of the load reactive power model, that is, $n_{ap} + n_{bp}$
The ordinate is the error sum of squares shown in formula (18).
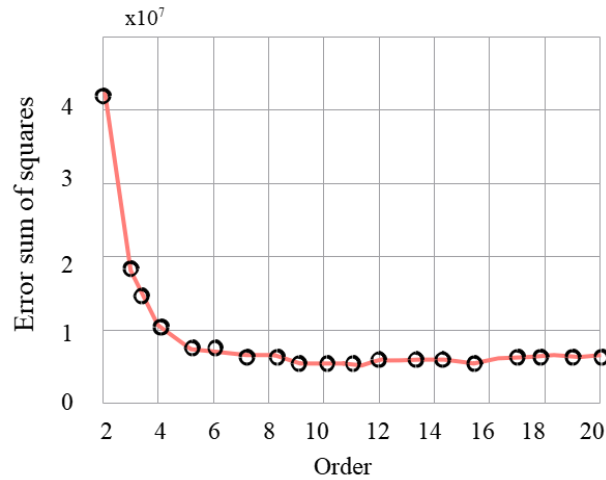

(a) Order selection of the load active power model
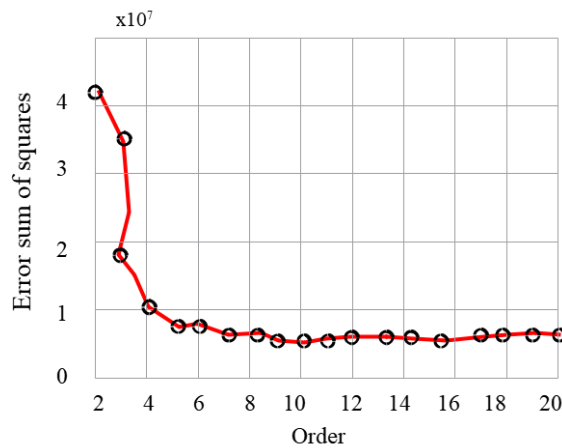
(b) Order selection of the load reactive power model

Figure 3: Relationship between load model order and error sum of squares.

It can be seen from Figure 3 that the optimal orders of the load active power model and the reactive power model are $n_{ap} + n_{bp} = 11$ and $n_{aq} + n_{bq} = 12$ respectively. However, when the order of the load model increases to $n_{ap} + n_{bp} = 5$ and $n_{aq} + n_{bq} = 4$, the error sum of squares does not decrease significantly, and even increases. This is because when the order of the identified load model is higher than the order of the real load model, numerical instability will occur. The inflection

point of the L-shaped curve is the order of the load model, and $n_{ap} = 4, n_{bp} = 1, n_{aq} = 3, n_{bq} = 1$ is obtained at this point by calculation. In the same way, the load model order of education branch system 2 and education branch system 3 can be obtained. The load model order of education branch system 2 is $n_{ap} = 5, n_{bp} = 1, n_{aq} = 4, n_{bq} = 1$, and the load model order of education branch system 3 is $n_{ap} = 3, n_{bp} = 2, n_{aq} = 5, n_{bq} = 1$.

The response output of the load BJ model is obtained from the input of the identification set and the simulation set, respectively, and is compared with the measured data of the PMU. Figure 4 is a fitting curve between the APRP response of the load model identified using the fifteenth group of data of the education branch system 1 and the APRP measured by the PMU. Figure 5 is the fitting curve between the APRP response of the load model identified using the 28th group data of the education branch system 2 and the APRP measured by the PMU. Figure 6 is a fitting curve between the APRP response of the load model identified using the fourth group of data of the education branch system 3 and the APRP measured by the PMU. They correspond to the data of the identification set $112s-116s$, $216s-220s, 24s-28s$, and the data of the verification set $116s-120s$, $220s-224s$, and $28s-32s$ respectively.
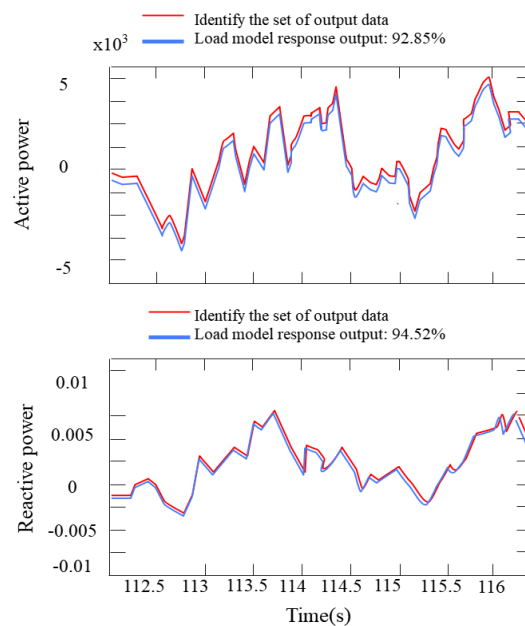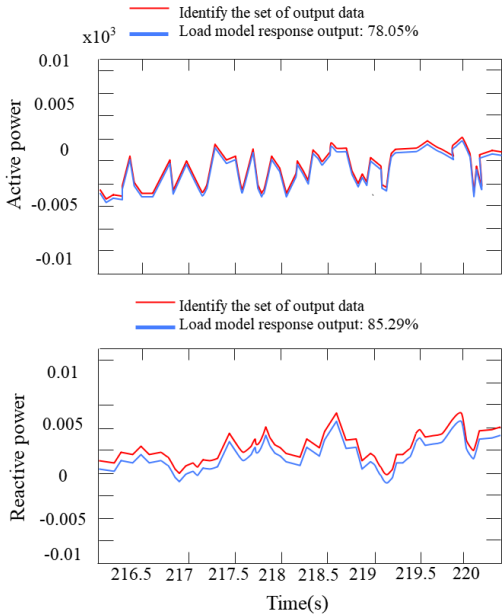

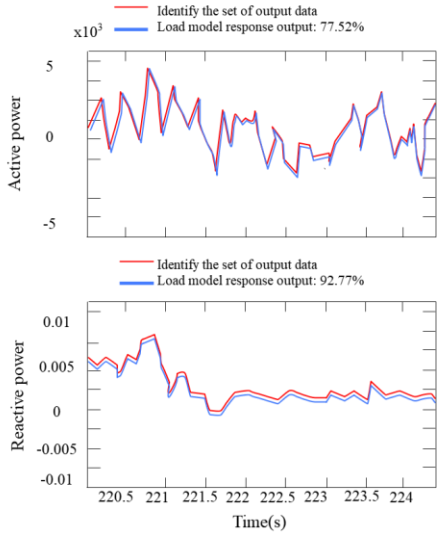(a) Fitting curve of the identification set data
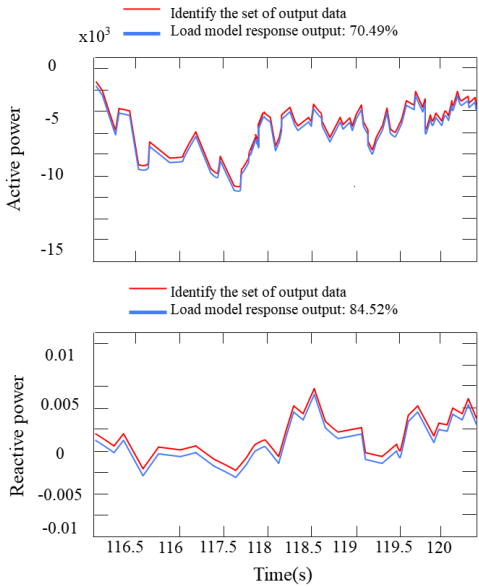
(b) Fitting curve of the simulated set data

Figure 4: Fitting curve of active and reactive power (AAP) response of load model and PMU measured AAP Experiment 1.
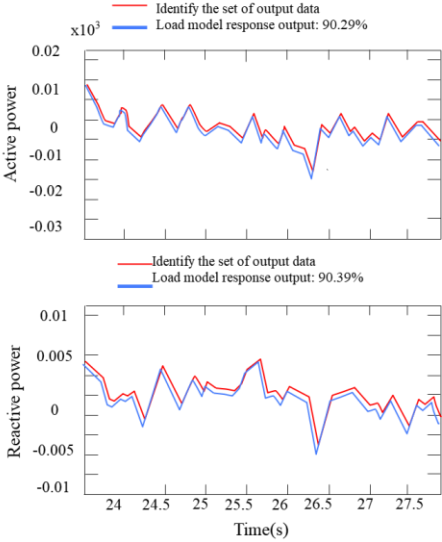

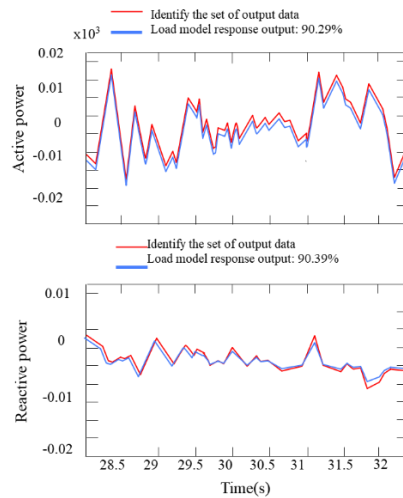(a) Fitting curve of the identification set data

(b) Fitting curve of the simulated set data

Figure 5: Fitting curve of AAP response of load model and PMU measured AAP Experiment 2.

(a) Fitting curve of the identification set data
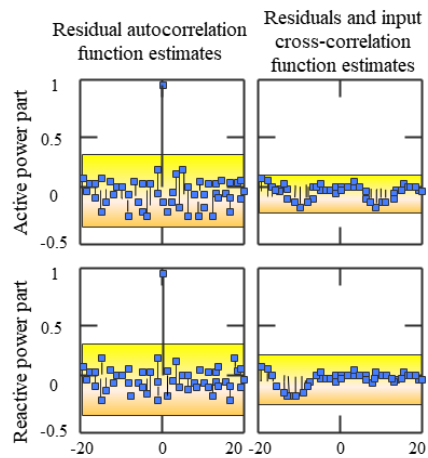
(b) Fitting curve of the simulated set data

Figure 6: Fitting curve of AAP response of load model and PMU measured AAP Experiment 3

The black curves in the above figure are the measured AAP values of the PMU, and the red curves are the AAP responses of the load model using the method proposed in this paper. It can be seen that with the method proposed in this paper, and the fitting degree of the measured data and the response output data of the identified load model can reach about 80%, which verifies the effectiveness of the method proposed in this paper.
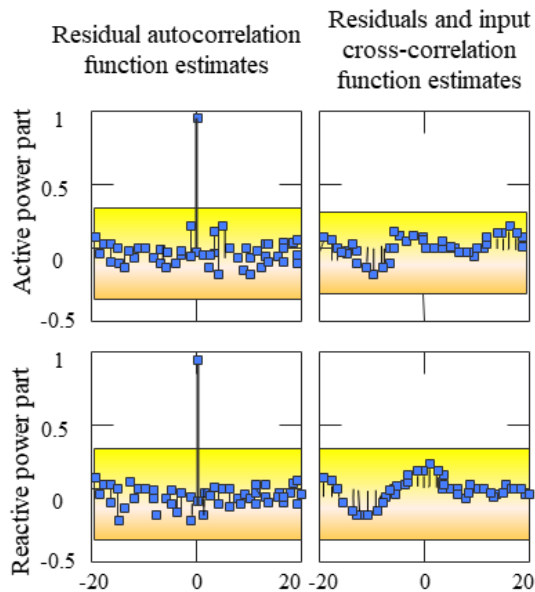
In addition, the whiteness test and the independence test are carried out on the residual between the response output of the identification load model and the measured data of the PMU, as shown in Figure 7.
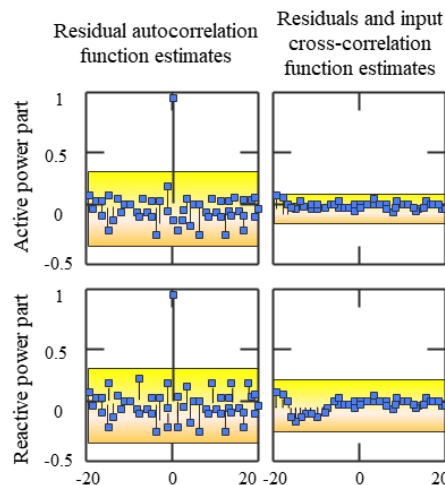
(a) Residual difference analysis of the Joaquin variable load model

Residual autocorrelation function estimates / Residuals and input cross-correlation function estimates

(b) Residual analysis of the Tai Zhen variable load model

Residual autocorrelation function estimates / Residuals and input cross-correlation function estimates

(c) Residual analysis of the Qing Yang variable load model

Figure 7: Residual analysis.

In Figure 7, the blue area is the confidence interval at the 99% confidence level. It can be seen that the autocorrelation function value of the residual is basically within the confidence interval at $\tau \neq 0$, that is, close to 0, so the residual is close to white noise. Similarly, the value of the cross-correlation function between the residuals and past inputs is basically within the confidence interval, that is,

close to 0, so the residuals and past inputs are independent. It shows that the load model established by the method proposed in this paper can accurately describe the load in the actual SES network. The practical effect evaluation of the SES based on the CCC task scheduling algorithm proposed in this paper is carried out, and the teaching simulation is verified, and the experimental results shown in the table below.

Num	Resource Scheduling	Num	Resource Scheduling	Num	Resource Scheduling
1	90.65	23	80.36	45	86.82
2	89.68	24	85.00	46	89.50
3	83.69	25	89.14	47	80.40
4	88.58	26	88.14	48	90.03
5	88.52	27	81.23	49	88.96
6	84.22	28	82.83	50	81.17
7	87.05	29	90.37	51	88.84
8	81.72	30	82.46	52	86.48
9	86.82	31	89.28	53	84.69
10	80.22	32	81.12	54	80.42
11	83.00	33	86.55	55	84.21
12	84.02	34	80.43	56	87.17
13	90.95	35	83.29	57	84.81
14	87.54	36	85.37	58	85.03
15	81.92	37	81.48	59	80.12
16	87.92	38	82.92	60	86.95
17	85.31	39	85.98	61	88.43
18	87.58	40	90.00	62	90.51
19	85.64	41	84.17	63	87.78
20	87.96	42	85.42	64	85.97
21	84.14	43	89.80	65	82.27
22	83.61	44	84.10	66	83.58

The above research shows that the SES based on the cloud-side collaborative computing task scheduling algorithm can effectively improve the effect of CCERS.

4   CONCLUSION

Education cloud can reduce the construction cost of educational resource platform. For example, it can aggregate educational resources, then reuse idle machines, and put various large-scale programs on the cloud. In this way, schools do not need to spend a lot on hardware purchases, nor do they need to invest a lot of energy in operation and maintenance. Instead, the efficiency of work and learning is continuously improved due to cloud technology. This paper combines the cloud collaborative computing task scheduling algorithm to carry out the resource scheduling processing of the smart education model. The experimental research shows that the SES based on the cloud-side collaborative computing task scheduling algorithm can effectively improve the effect of CCERS.

Guirong Li, https://orcid.org/0000-0002-1763-8188
Lei Shu, https://orcid.org/0009-0004-0826-2117

ACKNOWLEDGEMENT

REFERENCES

[1]   Alfalah, S. F.; Falah, J. F.; Alfalah, T.; Elfalah, M.; Muhaidat, N.; Falah, O.: A comparative study between a virtual reality heart anatomy system and traditional medical teaching modalities, Virtual Reality, 23(3), 2019, 229-234. https://doi.org/10.1007/s10055-018-0359-y

[2]   Andrunyk, V.; Shestakevych, T.; Pasichnyk, V.: The technology of augmented and virtual reality in teaching children with ASD, Econtechmod: Scientific Journal, 4 (7), 2018, 7(4), 2018, 59-64.

[3]   Bennie, S. J.; Ranaghan, K. E.; Deeks, H.; Goldsmith, H. E.; O'Connor, M. B.; Mulholland, A. J.; Glowacki, D. R.: Teaching enzyme catalysis using interactive molecular dynamics in virtual reality, Journal of Chemical Education, 96(11), 2019, 2488-2496. https://doi.org/10.1021/acs.jchemed.9b00181

[4]   Chang, P. W.; Chen, B. C.; Jones, C. E.; Bunting, K.; Chakraborti, C.; Kahn, M. J.: Virtual reality supplemental teaching at low-cost (VRSTL) as a medical education adjunct for increasing early patient exposure, Medical Science Educator, 28(1), 2018, 3-4. https://doi.org/10.1007/s40670-017-0483-4

[5]   Dayarathna, V. L.; Karam, S.; Jaradat, R.; Hamilton, M. A.; Nagahi, M.; Joshi, S.; Driouche, B.: Assessment of the efficacy and effectiveness of virtual reality teaching module: A gender-based comparison, International Journal of Engineering Education, 36(6), 2020, 1938-1955.

[6]   Dilmurod, R.; Fazliddin, A.: Prospects for the introduction of artificial intelligence technologies in higher education, ACADEMICIA: An International Multidisciplinary Research Journal, 11(2), 2021, 929-934. https://doi.org/10.5958/2249-7137.2021.00468.7

[7]   Guan, C.; Mou, J.; Jiang, Z.: Artificial intelligence innovation in education: A twenty-year data-driven historical analysis, International Journal of Innovation Studies, 4(4), 2020, 134-147. https://doi.org/10.1016/j.ijis.2020.09.001

[8]   Hernandez-Pozas, O.; Carreon-Flores, H.: Teaching international business using virtual reality, Journal of Teaching in International Business, 30(2), 2019, 196-212. https://doi.org/10.1080/08975930.2019.1663779

[9]   Huang, S.: Analysis of psychological teaching assisted by artificial intelligence in sports training courses, Journal of Applied Science and Engineering, 24(5), 2021, 743-748.

[10]   Lin, P. H.; Wooders, A.; Wang, J. T. Y.; Yuan, W. M.: Artificial intelligence, the missing piece of online education?, IEEE Engineering Management Review, 46(3), 2018, 25-28. https://doi.org/10.1109/EMR.2018.2868068

[11]   Mayne, R.; Green, H.: Virtual reality for teaching and learning in crime scene investigation, Science & Justice, 60(5), 2020, 466-472. https://doi.org/10.1016/j.scijus.2020.07.006

[12] McCool, K. E.; Bissett, S. A.; Hill, T. L.; Degernes, L. A.; Hawkins, E. C.: Evaluation of a human virtual-reality endoscopy trainer for teaching early endoscopy skills to veterinarians, Journal of veterinary medical education, 47(1), 2020,106-116. https://doi.org/10.3138/jvme.0418-037r

[13] Ni, D.: The application of artificial intelligence technology in international chinese language teaching, Chinese Journal of Social Science and Management, 5(1), 2021, 101-112.

[14] Ramlogan, R.; Niazi, A. U.; Jin, R.; Johnson, J.; Chan, V. W.; Perlas, A.: A virtual reality simulation model of spinal ultrasound: role in teaching spinal sonoanatomy, Regional Anesthesia & Pain Medicine, 42(2), 2017, 217-222. https://doi.org/10.1097/AAP.0000000000000537

[15] Reymus, M.; Liebermann, A.; Diegritz, C.: Virtual reality: an effective tool for teaching root canal anatomy to undergraduate dental students–a preliminary study, International Endodontic Journal, 53(11), 2020, 1581-1587. https://doi.org/10.1111/iej.13380

[16] Ribeiro, P.; Simões, H.; Ferreira, M.: Teaching artificial intelligence and logic programming in a competitive environment, Informatics in Education, 8(1), 2009, 85-100. https://doi.org/10.15388/infedu.2009.06

[17] Taubert, M.; Webber, L.; Hamilton, T.; Carr, M.; Harvey, M.: Virtual reality videos used in undergraduate palliative and oncology medical teaching: results of a pilot study. BMJ Supportive & Palliative Care, 9(3), 2019, 281-285. https://doi.org/10.1136/bmjspcare-2018-001720

[18] Xu, X.; Guo, P.; Zhai, J.; Zeng, X.: Robotic kinematics teaching system with virtual reality, remote control and an on–site laboratory, International Journal of Mechanical Engineering Education, 48(3), 2020, 197-220. https://doi.org/10.1177/0306419018807376

[19] Yang, R.: Artificial Intelligence-Based Strategies for Improving the Teaching Effect of Art Major Courses in Colleges, International Journal of Emerging Technologies in Learning (iJET), 15(22), 2020, 146-160. https://doi.org/10.3991/ijet.v15i22.18199

[20] Zhao; Huiliang; Jian Lyu; Xiang Liu; Zhenghong Liu: Customization-oriented product flexible manufacturing experience system design based on VR,In IOP Conference Series: Materials Science and Engineering, 561(1), 012098. IOP Publishing, 2019. https://doi.org/10.1088/1757-899X/561/1/012098